



Behavior of Slender GFRP Reinforced Concrete Columns

Koosha Khorramian, Ph.D. Candidate¹ and Pedram Sadeghian, Ph.D., P.Eng., M.ASCE²

¹Department of Civil and Resource Engineering, Dalhousie University, Halifax, Nova Scotia, Canada, B3H 4R2; e-mail: Koosha.khorramian@dal.ca

²Department of Civil and Resource Engineering, Dalhousie University, Halifax, Nova Scotia, Canada, B3H 4R2; e-mail: Pedram.Sadeghian@dal.ca

ABSTRACT

This paper presents an experimental and analytical study on slender concrete columns reinforced with glass fiber-reinforced polymer (GFRP) bars. The experimental program included ten concrete columns with rectangular cross-section (203×305 mm) where nine of them were reinforced with #6 GFRP bars and one of them was reinforced with steel rebars. Three different reinforcement ratios of 4.70, 2.82, and 2.04 as well as four slenderness ratios of 17, 22, 40, and 60 were considered under two load eccentricities of 0.1 and 0.25 of width of the cross-section. The analytical model considered the material nonlinearity as well as the geometric nonlinearity. The model was verified against an independent experimental program. The model showed that as the load eccentricity and slenderness ratio increase, the load capacity decreases and as the reinforcement ratios increases, the load capacity slightly increases which shows effectiveness of GFRP bars in compression.

KEYWORDS

Concrete, Slender, Column, GFRP, bar, Experimental, Analytical

<https://doi.org/10.1061/9780784482230.010>

INTRODUCTION

For new constructions, in situations where special requirements such as corrosion resistance or electromagnetic transparency is demanded, Glass fiber-reinforced polymer (GFRP) bars have been recognized as an ideal alternative for steel rebar. The high tensile strength of GFRP bars justifies their usage in slabs and beams, however, their application in compressive members have not been suggested by guidelines. It is believed that GFRP bars are not effective in load bearing capacity of the column and some guidelines such as ACI 440.1 (2015) in which the contribution of GFRP bars in compression is neglected. Other guidelines such as CAN/CSA S806 (2012) or fib Bulletin 40 (2007) mentioned the same restriction which requires the neglect of the GFRP bars in compression. According to researches performed by Choo et al. (2006) analytically and De Luca et al. (2010) experimentally the neglect of the compressive bars is conservative. However, Tobi et al. (2012) found that the contribution of GFRP bars and steel bars in concrete columns are very

close to each other. Hales et al. (2016) tested high strength slender concrete columns reinforced by GFRP bars and confined by GFRP spiral and found them an acceptable system. Furthermore, Mohamed et al. (2014), Khorramian and Sadeghian (2017a and 2017b), Fillmore and Sadeghian (2018) observed the compressive strain levels for GFRP bars in compression which were higher than the defined crushing strain of the concrete in compression. These contrasts arise from lack of experimental data base for GFRP reinforced concrete columns in comparison to the steel RC columns. The database is even smaller for slender concrete columns reinforced with GFRP bars although their importance is not less than short columns.

The slenderness limit for concrete columns reinforced with GFRP bars are less than steel RC columns. While ACI 318-14 (2014) established the critical slenderness ratio of 22 for steel RC columns, Mirmiran et al. (2001) proposed 17 and Zadeh and Nanni (2013) proposed 14 for critical slenderness ratio. The latter result in having more GFRP RC columns in the category of slender columns where the second order effects or large deformations cannot be neglected in the design procedure which emphasizes the importance of studying slender GFRP RC columns. The questions and doubts in compressive GFRP bars from one side, and the lack of experimental data for GFRP RC columns from the other side along with the importance of the slender category of these columns showed a critical demand to improve the experimental data base to perform investigation on the behavior of slender GFRP RC columns. The current study was designed to focus on the behavior of slender concrete columns reinforced with GFRP bars experimentally and to show how to model these columns analytically. In the experimental part, ten large-scale concrete columns reinforced with GFRP bar or steel bar with different slenderness ratios and reinforcement ratios were tested under eccentric loading up to failure.

EXPERIMENTAL PROGRAM

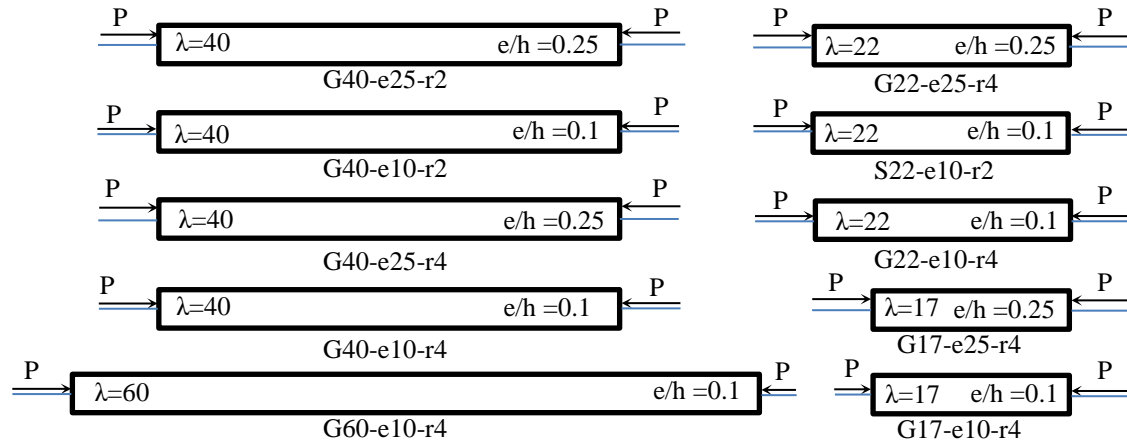
A total of ten large-scale reinforced concrete columns with rectangular cross section with different slenderness ratios were tested under eccentric loading up to failure. Nine specimens were reinforced with GFRP bars while one of them was reinforced with steel rebar. The experimental program consists of an explanation of the test matrix, material properties, fabrication and preparation, test set up and instrumentation as well as the results and discussion as presented in the following.

Test Matrix

In this study, a total of ten concrete columns with a rectangular cross section (203×305 mm) were prepared and tested under eccentric loading. Two different reinforcement ratios of 4.70, 2.82 were selected for concrete specimens reinforced with GFRP bars (corresponding to 10#6 and 6#6) while 2.04 was used for steel reinforced concrete (corresponding to 6-10M). Two different eccentricity to width ratios of 0.1 and 0.25 along with four slenderness ratios of 17, 22, 40, and 60 (four lengths of 1036, 1341, 2438, and 3657 mm) were formed different specimens as illustrated in Table 1 and Figure 1. The specimen ID for each specimen is built with a general form of “Aλ-eβ-rγ” in which A, λ, β, and γ present the type of reinforcement (G for Glass FRP and S for steel), slenderness ratio, eccentricity ratio, and reinforcement ratio, respectively, as shown in Table 1.

Table 1. Test matrix.

No.	Specimen ID	Slenderness ratio	Eccentricity ratio	Reinforcement ratio (%)	Reinforcement Type
1	G17-e10-r4	17	0.1	4.70	GFRP bar
2	G17-e25-r4	17	0.25	4.70	GFRP bar
3	G22-e10-r4	22	0.1	4.70	GFRP bar
4	G22-e25-r4	22	0.25	4.70	GFRP bar
5	S22-e10-r2	22	0.1	2.04	Steel rebar
6	G40-e10-r2	40	0.1	2.82	GFRP bar
7	G40-e25-r2	40	0.25	2.82	GFRP bar
8	G40-e10-r4	40	0.1	4.70	GFRP bar
9	G40-e25-r4	40	0.25	4.70	GFRP bar
10	G60-e10-r4	60	0.1	4.70	GFRP bar

**Figure 1. Test specimen types.**

Material Properties

In this study, #6 GFRP bars were used to reinforce concrete columns. The diameter of bars and nominal cross-sectional area of bars were 19 mm and 285 mm², respectively. Moreover, the guaranteed tensile strength, the tensile modulus of elasticity, and ultimate strain of bars were reported by manufacturer as 690 MPa, 46 GPa, and 0.0149 mm/mm, respectively. For steel bars, the nominal diameter, and cross-sectional area were reported as 11.3 mm and 100 mm², respectively. Furthermore, the guaranteed tensile strength, the tensile modulus of elasticity, and ultimate strain of steel rebars were reported by manufacturer as 400 MPa and 200 GPa, respectively. In addition, a ready-mix concrete with maximum aggregate size of 12 mm and a slump of 200 mm were poured in place. The strength of concrete was recognized as 48 MPa by averaging the compressive strength of three 150×300 mm concrete cylinders at 28 days.

Fabrication and Preparation

The concrete specimens were prepared using wooden molds and pouring concrete in place. Figure 2(a) presents the wooden mold (203 × 305 mm) in which all sides were solid due to the application of the wooden stiffeners. The corners of specimens were chamfered by providing four triangular wooden sticks with a leg width of 25.4 mm) installed in four corners of the mold longitudinally. The bars cages were assembled using wooden parts in between the bars to keep the distance of bars consistent for all specimens as shown in Figure 2(b). For longitudinal reinforcement, #6 GFRP bars or 10M steel reinforcing bars were installed in two layers while for transverse reinforcement, #3 GFRP bars were opted for all specimens. To support the longitudinal bars, four premanufactured U-shape stirrups form two closed GFRP ties whose center to center spacing was 150 mm at the middle of the column. For the ends of the column, the spacing of GFRP ties reduced to 75 mm to strengthen those regions and to avoid the premature failure near the points on which concentrated loads are more effective.

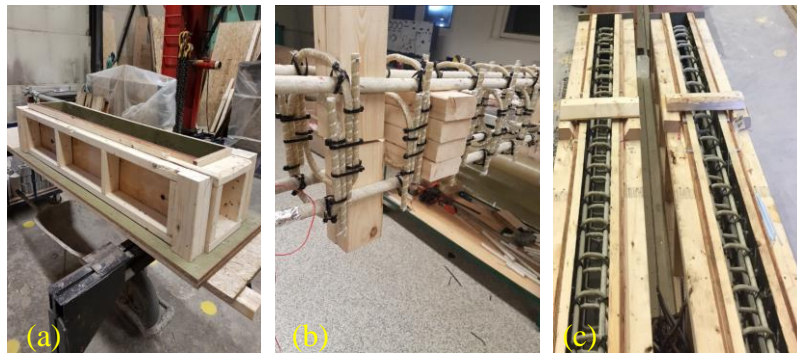


Figure 2: Specimen preparation: (a) molds, (b) bar cages, and (c) bar cages in molds - Courtesy of Koosha Khorramian.

The concrete cover of 25.4 mm from each side of the specimens was provided using proper plastic spacers at the bottom and sides of the molds measuring from top surface of the ties. The prepared specimens before pouring concrete are shown in Figure 2(c). The whole interior surface of the molds was lubricated by applying oil on the plywood and grease on the surface of chamfers. The sides of concrete specimens were restricted against slide by nailing some wooden parts on the top of each mold. The wire of strain gauges installed on the surface of longitudinal GFRP bars were protected against fresh concrete pressure and accidental damages by providing proper sleeve for them. The slump of concrete increased up to 200 mm using superplasticizer to the ready-mix concrete. The finished surface of the fresh concrete is shown in Figure 3(a). After pouring concrete, the surface of concrete specimens was covered with plastic sheets and were enclosed to save the moisture. After the fresh concrete set, the surface was covered with burlap [as shown in Figure 3(b)] and curing performed over seven days by keeping the plastic covers on them. Since the seven-day strength of concrete cylinders were higher than the expected value, after seven days, the curing was stopped in order not to gain extra strength due to capacity limit of testing device. The concrete specimens are shown in Figure 3(c). In order to strengthen the specimens at the ends of specimens and to prevent premature failure, two layers of epoxy resin and GFRP fabric, with a width of 200 mm, were wrapped at the ends of each specimen.

Instrumentation and Test Set-up

The experimental tests of large-scale concrete specimens were conducted using the test set up whose schematic configuration is shown in Figure 4. It is noticed that the columns were tested horizontally due to height limitation in the lab. The columns were tested under pin-pin boundary condition and combined axial and flexural loading. The test set-up elements included “Rod-End”, shaft, Tunnel, Concrete block, load cell, actuator, and swivel. To provide specimens with simply supported condition, at both ends of specimens there was a system of steel plates and cylinders called “Rod-End” in this paper. The Rod-End consisted of two steel plates which one of them attached to the concrete block (or the end of the shaft) and the other one was connected to the concrete column, a steel cylinder, and a thick steel plate with a V-shape notch. In Rod-End, between those two plates, there was a steel cylinder, welded and fixed to the plate which attached to the concrete block (or the end of the shaft), and a thick V-notched steel plate welded to the plate which was in contact with the specimen. The contact area of the V-notched plate and steel cylinder were greased properly which provided rotation for the column, and the location of the V-notched plate defined the load eccentricity. In other words, by removing the welds from the V-notched plate and change the position of that on the plate connected to column, the load desired load eccentricity achieved. Moreover, at the ends of columns, the wrapped ends of columns were tightly tied to the Rod-End by a system of steel plates as shown in Figure 4. The shaft consists of some steel plates which were welded to each other and form a solid steel box whose function was to apply the load indirectly to the specimen and protect the load cell. In order for shaft to be moved in the straight direction, the steel tunnel as a guide were installed on the floor which eliminates prevents the bending of the lateral movement of the shaft. To hold the system of swivel, actuator, and load cell and to provide a situation for applying load, two high strength steel reinforced concrete blocks were fixed to the concrete floor using bolts.



Figure 3. Concrete columns: (a) fresh concrete, (b) curing, and (c) concrete specimens - Courtesy of Koosha Khorramian.

A data acquisition system obtained the data with a frequency of 10 point per second capturing the values of eight strain gauges, six linear potentiometers (LPs), stroke displacement, and the applied load. The location of the strain gauges and LPs are presented in Figure 5. At the middle of each specimen, there were four strain gauges on the exterior surface of the longitudinal reinforcing bars as shown in section A-A in Figure 5. In addition, two other strain gauges were installed on the middle bars at sections whose distance from center was 200 mm, as indicated in Figure 5. To capture the rotation of the column ends, two LPs were installed at the ends of the columns as shown Figure 5. The displacement at the middle of the column specimen captured

using two LPs at the middle of the columns. The load applied to the specimen using displacement control approach with a rate of 1 mm/min using an actuator whose capacity was 2 MN.

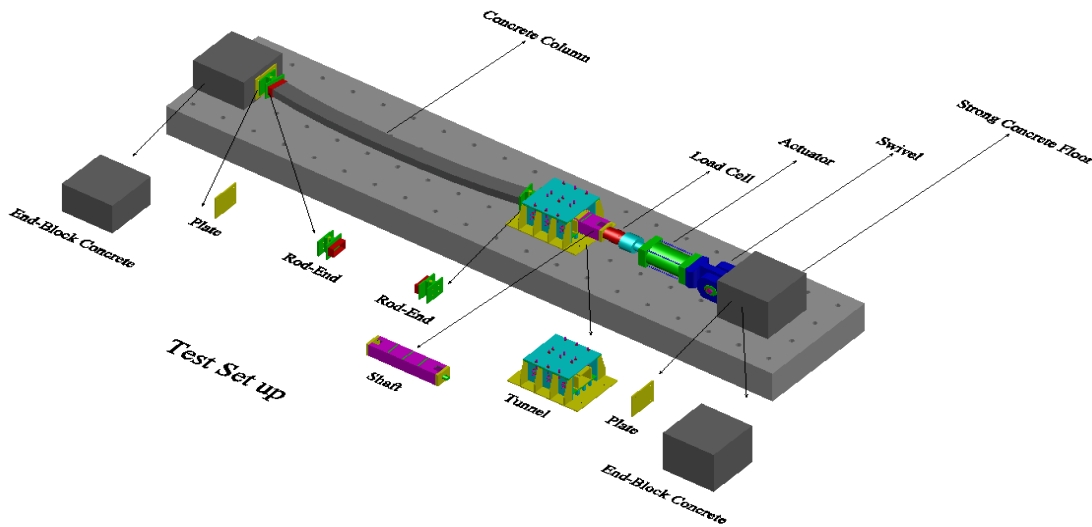


Figure 4. Schematic test set up.

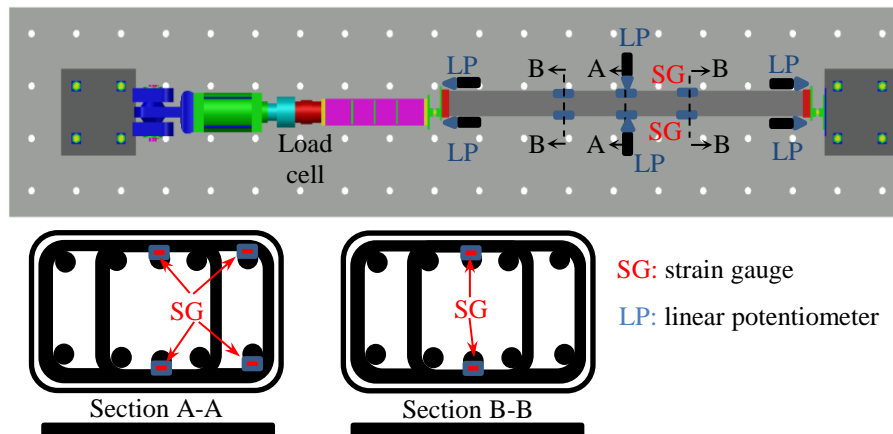


Figure 5. Instrumentation.

Results and Discussion

Figure 6 presents the failure of the specimen G22-e25-r4. The failure occurred at the middle of the specimen as shown in Figure 6(b) which shows that the test fixture worked properly. At the peak load, the failure happened as the concrete crushed in the compression side as presented in Figure 6(c). It should be noted that tensile cracks were observed in the tensile side of the specimen as shown in Figure 6(d). After crushing of concrete, the load in the system dropped as the displacement increased. However, after a certain amount of drop in the load, the specimen was able to tolerate a constant load as the loading continued through increasing the axial displacement, as observed in Figure 7 and Figure 8. The latter can be justified by the effect of compressive bars in compression which makes the column sustain load even after compressive concrete is crushed.

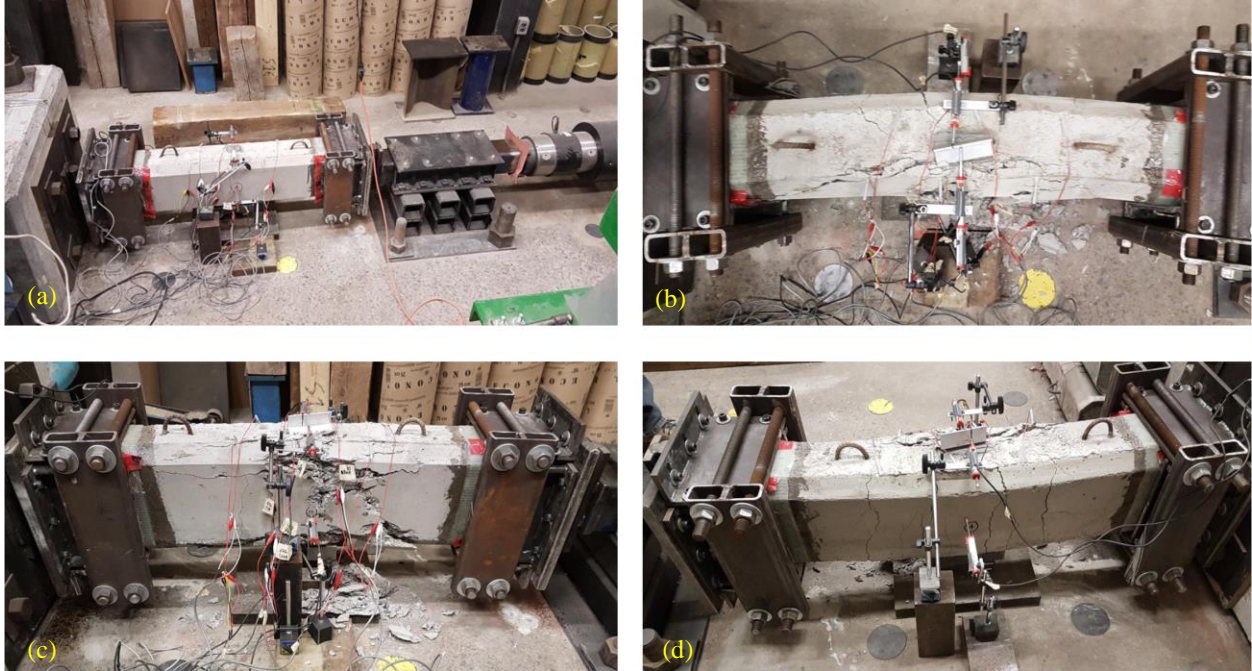


Figure 6. Concrete column failure: (a) specimen before testing, (b) top view, (c) compression side view, and (d) tension side view - Courtesy of Koosha Khorramian.

It was observed that the load capacity of specimen G22-e25-r4 was more than G17-e25-r4 which was not expected. It should be noted that specimen G17-e25-r4 was tested multiple times up to 1MN load but failed since its ends were failed due to lack of rigidity in the steel cap. The issue was solved by adding a solid steel belt to both ends of the specimen. However, testing multiple times had adverse effect in the ultimate load carrying capacity of G17-e25-r4. The other reason is that the strain difference in SG#2 and SG#4 is more considerable for G17-e25-r4 than for G22-e25-r4 that shows the bars were not in the same row for G17-e25-r4 which led to lower capacity.

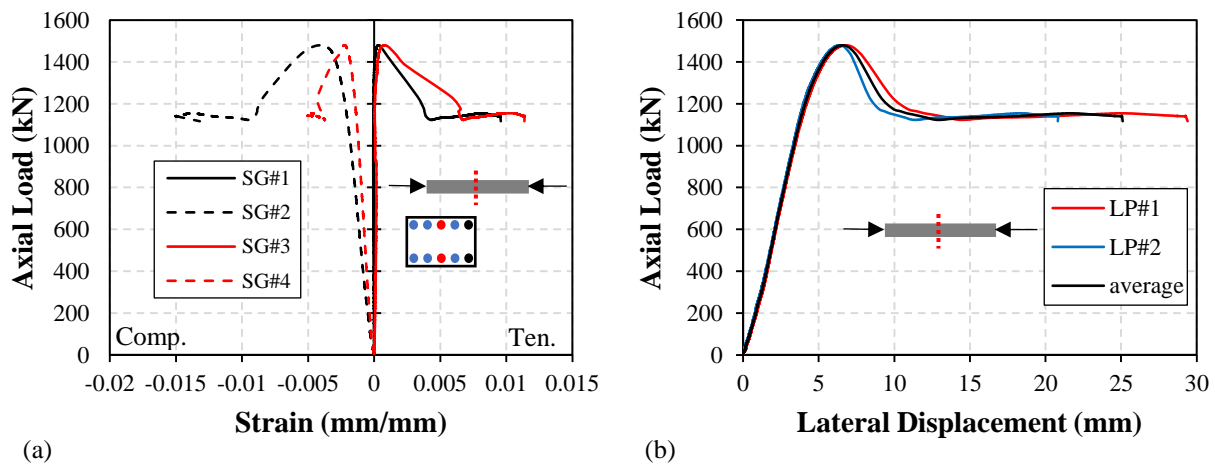


Figure 7. Test results for specimen G17-e25-r4: (a) load-strain at middle section, and (b) load-lateral displacement at the middle section.

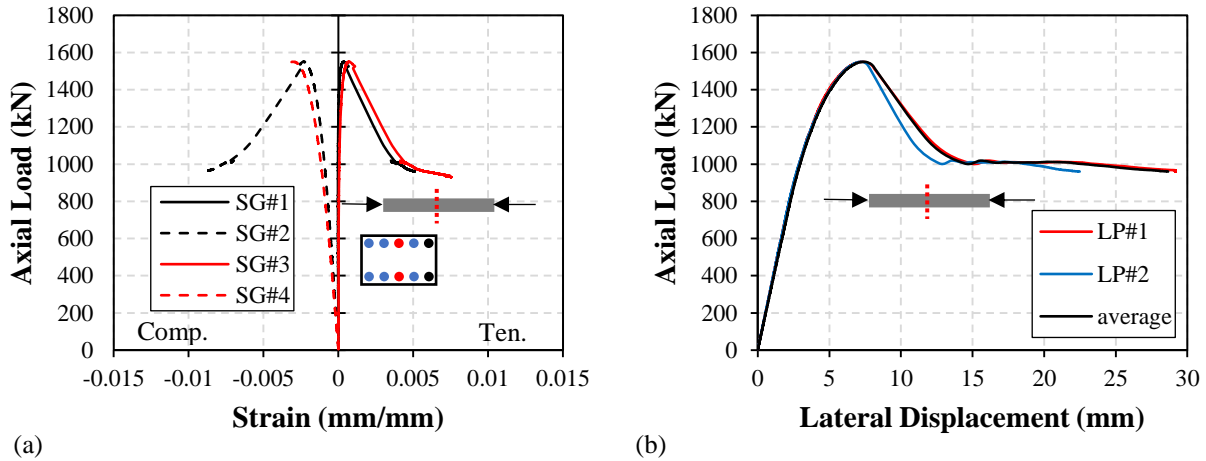


Figure 8. Test results for specimen G22-e25-r4: (a) load-strain at middle section, and (b) load-lateral displacement at the middle section.

NUMERICAL STUDY

This section presents an analytical approach to model the behavior of the slender concrete columns reinforced with GFRP bars as described in the previous section. The model considers second order effects as well as the material nonlinearity and is verified against an independent test result.

Model description

To study the behavior of concrete columns reinforced with GFRP, the columns were divided into three points, one at the middle of the column and two at the ends of the column. The characteristics of the columns such as displacement at middle of the column and the corresponding bending moment as well as the compressive and tensile strain of the GFRP bars were determined at different load levels. Using an iterative method for each load step, the displacement of at the middle section of the column was determined by finding the displacement which satisfies the sine shape assumption of the deflected shape of the column. Sadeghian and Fam (2015) used the idea of the sine function to derive the descending branch of load-displacement curves. The curvature function assumed to be a sine function in the length of the column which causes sine-shape deflected shape of the column using double integration from the curvature function. In each load step, the value of the displacement assumed at the middle, and the values of corresponding moments at the middle height of column, which is the axial load times the initial eccentricity plus the displacement, was calculated. This moment along with the end moments, which were determined by multiplying the axial load by the initial eccentricity, were used to determine the corresponding curvatures from the moment-curvature diagram of the section at that load step as illustrated in Figure 9.

To find the moment-curvature of column at each load step, each concrete section was discretized into rectangular fibers with a height of 0.25 mm in order to calculate the stress at the center of each fiber. The strain variation in the section was assumed linear, and the stress strain relationship of GFRP bars was considered linear up to failure while for concrete the nonlinear Popovics (1973) stress strain curve was considered. It was noted that the stress of concrete in tension was neglected. At a certain load, the curvature of the section varied by alteration of the values of the furthest compressive concrete fiber and calculating the depth of neutral axis from

satisfying the force equilibrium. By satisfying the moment equilibrium at each section the required load eccentricity was determined and, in turn, the corresponding moment to each imposed curvature as illustrated in Figure 10.

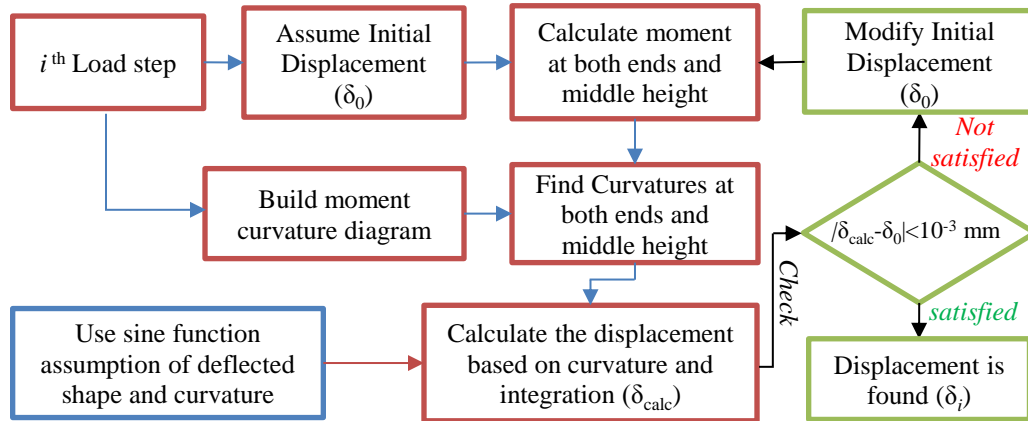


Figure 9. illustration of the numerical procedure for a certain load step.

Once the curvatures corresponding to the moments caused by the assumed displacement were found from the moment-curvature diagram, these curvatures were used to find the new displacement at the middle of the column. If the new displacement was closer than 0.001 mm to the initial assumed displacement, the found displacement considered as the converged value for that step, otherwise the iteration continues by changing the displacement to achieve convergence. The mentioned process continues by increasing the load up to a stage at which the moment corresponding to the converged middle height displacement of column required to be greater than the peak moment in the moment curvature diagram. After this peak load, a descending branch was investigated using the same procedure and logic by reducing the load while searching for converged displacements that increased in each step as the load decreases. A more comprehensive explanation and verification of the model with small scale columns could be found in an earlier study conducted by the authors (Khorramian and Sadeghian 2017-1).

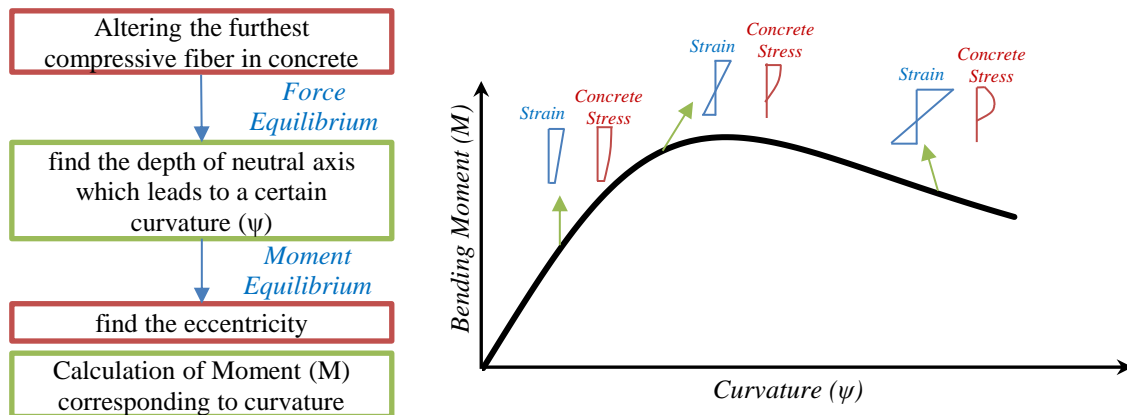


Figure 10. Moment curvature diagram for a certain load step.

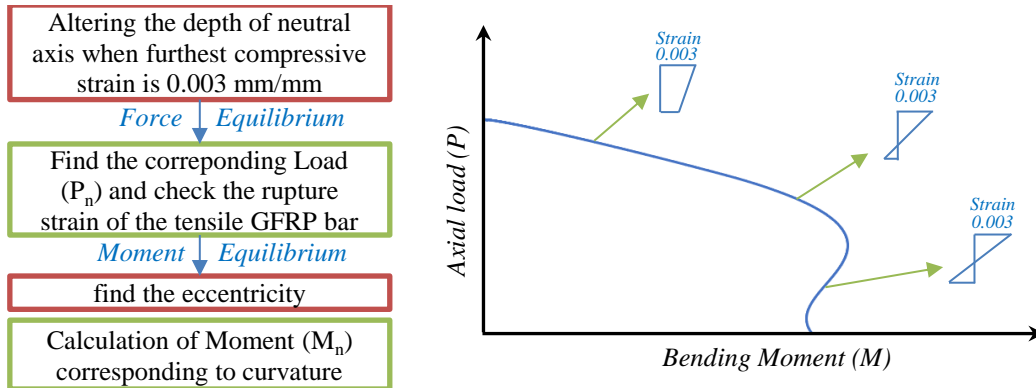


Figure 11. Bending moment-axial load interaction diagram.

It is noticed that the bending moment-axial load interaction diagram was derived using a similar procedure for finding the moment-curvature with the difference that the ultimate compressive fiber was considered as a constant value of 0.003 mm/mm according to ACI 318-14 (2014). Then by changing the depth of neutral axis and satisfying equilibrium equations in the section, the corresponding load and bending moment, or load eccentricity, was determined for as many points as needed to drive the diagram, as shown in Figure 11. Moreover, the tensile strain of bars was checked versus the tensile rupture strain of GFRP material at each step. For the steps at which the tensile strain of the GFRP bars reached the maximum value, instead of having the furthest compressive strain as 0.003 mm/mm, this value is allowed to change while the tensile strain of GFRP bars were constant and set to the rupture strain. It is noticed that for the current research, all points in the interaction diagrams were derived by setting the furthest strain as 0.003 mm/mm since the tensile strains of the GFRP bars did not reach their rupture values.

Model Verification

The model was verified versus an experimental study performed by Hadhood et. al (2017) in which four circular concrete columns reinforced with eight #5 GFRP bars with slenderness ratios of 20, length of 1500 mm, and diameter of 305 mm were considered. Column labels C2-P2, C3-P2, C4-P2, and C5-P2 presents 25, 50 100, and 200 mm eccentricities, respectively. The results showed a good agreement between the experimental and model as presented in Figure 12.

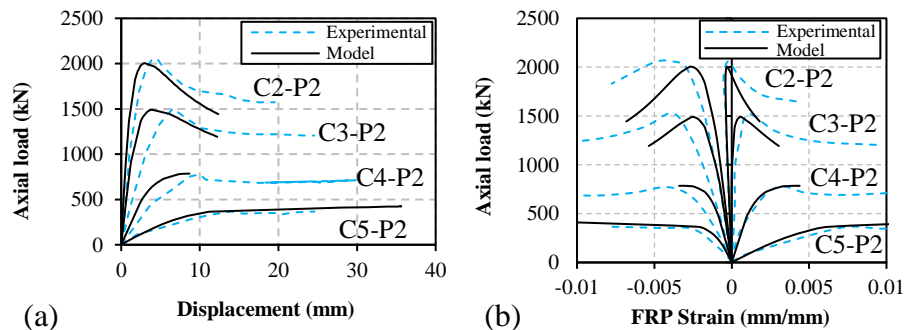


Figure 12. Model verification against test data by Hadhood et. al (2017) with slenderness ratios of 20: (a) load displacement, and (b) load strain of FRP bars.

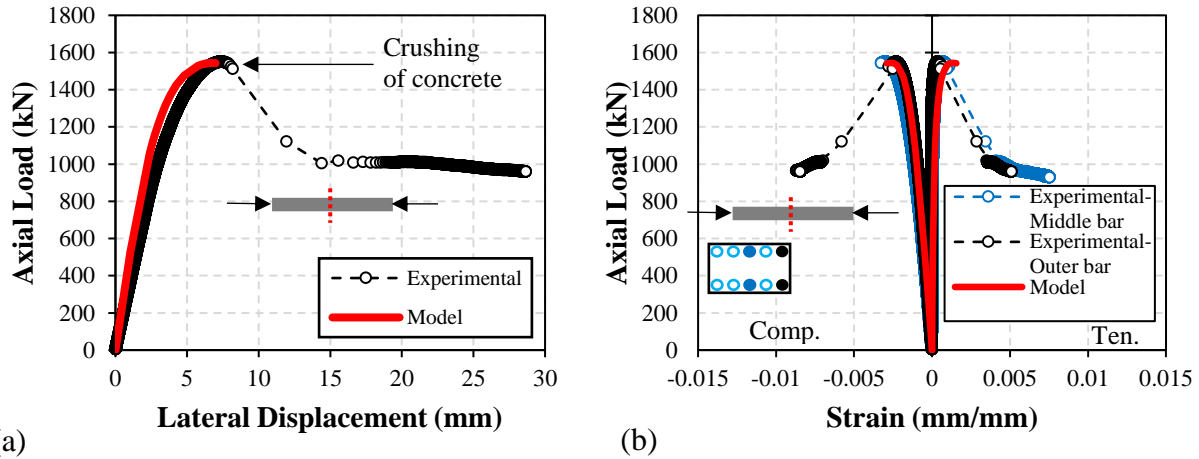


Figure 13. Model verification for G22-e25-r4: (a) load displacement, and (b) load strain of FRP bars.

The model verification is presented in Figure 13 for specimen G22-e25-r4. It should be noted that the effect of chamfers was considered in the calculations. The results show a well agreement between the experimental results and the model prediction. It should be noted that after peak load, there was a sudden drop in load and the specimen was crushed. Therefore, the model was able to predict the results only up to the failure point.

Parametric Study

Using the experimental dimensions and material properties presented in the experimental program and the procedure explained above, the loading path of the test specimens as well as the load displacement behavior of GFRP reinforced concrete columns, with slenderness ratio of 17, 22, 40, and 60 loaded with 0.1 eccentricity to width ratio, are presented in Figure 14. The results showed that as the slenderness ratio increases, the mode of failure changes from material failure to stability failure, the load carrying capacity decreases, and the second order effect increases.

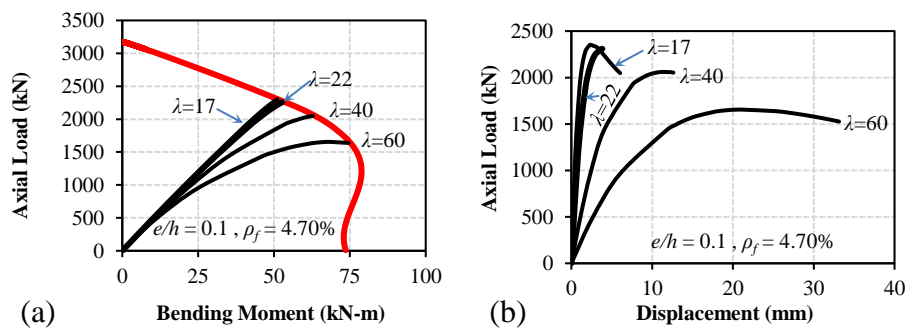


Figure 14. Parametric study: (a) loading path, and (b) load-displacement.

Conclusion

In this study, the behavior of slender GFRP reinforced concrete columns were evaluated. A total of ten large-scale concrete columns including nine GFRP reinforced and one steel reinforced concrete columns were prepared to be tested under eccentric loading and with a simply supported

boundary condition at both ends. Four slenderness ratios of 17, 22, 40, and 60 were considered as well as two eccentricity to width ratios of 0.1 and 0.25 while the reinforcement ratios varied as 4.7, 2.82, and 2.04 percent. The results showed that the GFRP reinforced concrete columns were able to sustain load even after compressive crushing of concrete. In addition to the experimental program, an analytical program was introduced in this paper in order to model the test specimens. According to the analytical model, the results showed that as the slenderness ratio increases, the mode of failure changes from material failure to stability failure, the load carrying capacity decreases, and the second order effect increases.

ACKNOWLEDGEMENT

Authors would like to thank Blair Nickerson, Brian Kennedy, Jesse Keane, Daina MacEachern, Mostafa Jafarian Abyaneh, Kumari Bandarage, Krishna Priyanka Garikapati, and Dillon Betts of Dalhousie University for their assistance in the lab. The authors would also like to acknowledge and thank Aslan FRP for providing the GFRP bars and Dalhousie University and the Natural Sciences and Engineering Research Council of Canada (NSERC) for their financial support.

REFERENCES

- ACI 318-14. (2014). "Building Code Requirements for Structural Concrete", Farmington Hills, MI: *American Concrete Institute*.
- ACI 440.1R. (2015). "Guide for the Design and Construction of Structural Concrete Reinforced Fiber-Reinforced Polymer (FRP) Bars", Farmington Hills, MI: *American Concrete Institute*.
- CAN/CSA S806-12 (2012). "Design and construction of building structures with fibre-reinforced polymers", *Canadian Standards Association*.
- Choo, C. C., Harik, I. E., and Gesund, H., (2006). "Strength of Rectangular Concrete Columns Reinforced with Fiber-Reinforced Polymer Bars", *ACI Structural Journal*, 103(3), 452-459.
- De Luca, A., Matta, F., and Nanni, A. (2010). "Behavior of Full-Scale Glass Fiber-Reinforced Polymer Reinforced Concrete Columns under Axial Load", *ACI Structural Journal*, 107(5), 589-596.
- Fillmore, B. and Sadeghian, P. (2018). "Contribution of longitudinal glass fiber-reinforced polymer bars in concrete cylinders under axial compression", *Canadian Journal of Civil Engineering*, 45, 458-468.
- Fib Bulletin 40 (2007). "FRP Reinforcement in RC structures", *The International Federation for Structural Concrete*, Stuttgart.
- Hales, T. A., Pantelides, C. P., and Reaveley, L. D. (2016). "Experimental Evaluation of Slender High-Strength Concrete Columns with GFRP and Hybrid Reinforcement", *Journal of Composites for Construction*, 20(6), 04016050.
- Hadhood, A., Mohamed, H. M., Ghrib, F., and Benmokrane, B. (2017). "Efficiency of glass-fiber reinforced-polymer (GFRP) discrete hoops and bars in concrete columns under combined axial and flexural loads", *Composites Part B*, 114, 223-236.
- Khorramian, K. and Sadeghian, P. (2017a). "Experimental and analytical behavior of short concrete columns reinforced with GFRP bars under eccentric loading", *Engineering structures*, 151, 761-773.

- Khorrarnian, K. and Sadeghian, P. (2017b). "Short Concrete Columns Reinforced with GFRP Rebars under Eccentric Loading" *CSCE Annual Conference*, Vancouver, BC, Canada.
- Mirmiran, A., Yuan, W., and Chen, X. (2001). "Design of Slenderness in Concrete Columns Internally Reinforced with Fiber-Reinforced Polymer Bars", *ACI Structural Journal*, 98(1), 116-125.
- Mohamed, H. M., Afifi, M. Z., and Benmokrane, B. (2014). "Performance Evaluation of Concrete Columns Reinforced Longitudinally with FRP Bars and Confined with FRP Hoops and Spirals under Axial Load", *Journal of Bridge Engineering*, 19(7), 04014020.
- Popovics, S. (1973). "A numerical approach to the complete stress-strain curve of concrete", *Cement and concrete research*, 3(5), 583-599.
- Sadeghian, P. and Fam, A. (2015). "Strengthening Slender Reinforced Concrete Columns Using High-Modulus Longitudinal Reinforcement for Buckling Control", *Journal of Structural Engineering, ASCE*, 141(4), 04014127.
- Tobbi, H., Farghaly, A.S., and Benmokrane, B. (2012). "Concrete Columns Reinforced Longitudinally and Transversally with Glass Fiber-Reinforced Polymer Bars", *ACI Structural Journal*, 109(4), 551-558.
- Zadeh, H. J. and Nanni, A. (2013). "Design of RC Columns Using Glass FRP Reinforcement", *Journal of Composites for Construction*, 17(3), 294-304.